NUCLEAR ENERGY DENSITY FUNCTIONALS AND NEUTRON STAR PROPERTIES*

N. Paar[a,b], Ch.C. Moustakidis[c], G.A. Lalazissis[c]
T. Marketin[b], D. Vretenar[b]

[a]Department of Physics, University of Basel
Klingelbergstrasse 82, 4056 Basel, Switzerland
[b]Department of Physics, Faculty of Science, University of Zagreb
Bijenička 32, 10000 Zagreb, Croatia
[c]Department of Theoretical Physics, Aristotle University of Thessaloniki
54124 Thessaloniki, Greece

(Received January 12, 2015)

Recently, a method based on relativistic nuclear energy density functional (EDF) has been employed to study relations between collective excitations in finite nuclei with the nuclear matter symmetry energy, and the phase transition density n_t and pressure P_t at the inner edge separating the liquid core and the solid crust of a neutron star. By using the thermodynamic method, relativistic EDF and experimental data on the properties of charge-exchange dipole transitions, isovector giant dipole and quadrupole resonances and pygmy dipole transitions, the neutron star liquid-to-solid phase transition density and pressure are constrained. The analysis shows that accurate measurements are necessary to further constrain the symmetry energy parameters and the structure of neutron star crust.

DOI:10.5506/APhysPolB.46.369
PACS numbers: 26.60.+c, 24.30.Cz, 21.60.Jz, 21.65.Ef

1. Introduction

The composition of the crust of a neutron star presents an interesting challenge both for nuclear structure physics as well as for astrophysics. Since the crust represents an interface between observable surface phenomena and the invisible core of the star, its structure can be related to various interesting effects, such as glitches in the rotational period of pulsars, thermal relaxation after matter accretion, quasi periodic oscillations and anisotropic

* Presented at the Zakopane Conference on Nuclear Physics "Extremes of the Nuclear Landscape", Zakopane, Poland, August 31–September 7, 2014.

surface cooling [1]. The solid crust of thickness ≈ 1 km, composed of nonuniform neutron-rich matter is located above a liquid core [2]. The inner crust comprises the region from the density at which neutrons drip out from nuclei, to the inner edge separating the solid crust from the homogeneous liquid core. Due to rather limited knowledge of the equation of state of neutron-rich nuclear matter, the transition density at the inner edge is rather uncertain quantity. Among the key properties of neutron stars are the phase transition density $n_{\rm t}$ and pressure $P_{\rm t}$ at the inner edge separating the liquid core and the solid crust. The quantities such as $n_{\rm t}$ and $P_{\rm t}$, that determine the core-to-crust phase transition, play an important role in connecting the properties of the interior of neutron star with observable phenomena.

As pointed out in a number of previous studies, the core-crust transition density and pressure are highly sensitive to the poorly constrained density dependence of the nuclear matter symmetry energy [3–6]. It is important to note that the symmetry energy that governs the composition of the neutron star crust also determines the thickness of the neutron-skin $r_{np} = r_n - r_p$ in finite nuclei. In Ref. [3], an inverse correlation was found between the liquid-to-solid phase transition density for neutron-rich matter and the neutron-skin thickness of ^{208}Pb. Additional correlations between r_{np} and neutron star properties have also been investigated [7], including neutron star radii [8], the threshold density at the onset of the direct Urca process [9], and the crustal moment of inertia [7, 10]. More recent study based on nuclear energy density functionals and covariance analysis provides an insight into correlations between r_{np} and a variety of neutron star properties [11]. As pointed out in Ref. [3], an accurate measurement of the neutron radius of ^{208}Pb by means of parity-violating electron scattering may have important implications for the structure of the crust of neutron stars. However, recent parity violating electron scattering experiment on ^{208}Pb resulted in rather large experimental uncertainty of the neutron skin thickness ($r_{np} = 0.33^{+0.16}_{-0.18}$ fm) [12]. On the other hand, recent experiment based on coherent pion photoproduction resulted with $r_{np} = 0.15 \pm 0.03({\rm stat})^{+0.01}_{-0.03}({\rm syst})$ [13], similar to the value deduced from antiprotonic atoms, $r_{np} = 0.16 \pm 0.02({\rm stat}) \pm 0.04({\rm syst})$ [14].

The focus of the current study is to investigate additional experimental constraints for neutron star properties that could be gained from the studies of finite nuclei. Recently, we have introduced an alternative method to determine neutron star core-to-crust transition density and pressure by using collective excitations in finite nuclei that provide constraints on the symmetry energy and correlate with r_{np} [15]. Over the past years, experimental studies of giant resonances, pygmy dipole transitions and other modes of excitation in nuclei, yielded a wealth of data that constrain the nuclear symmetry energy and neutron skin thickness [16]. Since there is a direct relation between the liquid-to-solid transition density and the neutron radius

of ^{208}Pb [3], an analysis of the collective response of finite nuclei could also provide useful information about the crust of neutron stars. We show that by employing the framework that includes the thermodynamic method and relativistic nuclear energy density functional, one can analyze the properties of collective modes of excitation in finite nuclei, and establish constraints on the symmetry energy parameters and neutron star properties.

In Sec. 2 a theory framework is briefly introduced. Constraints from the model calculations and experimental data on the symmetry energy parameters are given in Sec. 3, while Sec. 4 contains the results on the neutron star liquid-to-solid transition density and pressure. The concluding remarks are given in Sec. 5.

2. Symmetry energy and neutron star properties

The equation of state of nuclear matter can be approximated as the sum of the energy per nucleon of symmetric matter and an asymmetry term [17]

$$E(n,\delta) = E_{\rm SNM}(n,0) + E_{\rm sym}(n)\delta^2\,, \tag{1}$$

where $\delta = (n_n - n_p)/n$ is the asymmetry, and n_n,n_p, and n denote the neutron, proton, and nucleon densities, respectively. The density dependence of the symmetry energy $E_{\rm sym}(n)$ can be expressed in terms of coefficients of a Taylor expansion around nuclear matter saturation density n_0

$$E_{\rm sym}(n) = E_{\rm sym}(n_0) + L\left(\frac{n-n_0}{3n_0}\right) + \dots\,, \tag{2}$$

where $E_{\rm sym}(n_0) \equiv J$ is the symmetry energy at saturation, and L denotes the slope parameter. It has been shown that the parameters J, L correlate not only with the neutron-skin thickness of nuclei [18, 19], but also with neutron star properties [11, 20]. The slope parameter is of a particular importance because it governs the pressure of the symmetry energy in pure neutron matter at n_0. It is the same pressure that pushes the neutrons against the surface tension in finite nuclei, determines the neutron-skin thickness and also supports a neutron star against gravity. Therefore, it is essential to provide accurate estimates of the symmetry energy parameters. Possible constraints on J and L from collective modes of excitation in finite nuclei are discussed in Sec. 3.

The present analysis is also focused on the properties of neutron stars, in particular, the liquid-to-solid transition density $n_{\rm t}$ and pressure $P_{\rm t}$ for neutron-rich matter. The usual approach to determine $n_{\rm t}$ is to find the density at which the uniform liquid becomes unstable against small-amplitude density fluctuations, indicating the formation of nuclear clusters. In this way,

a lower bound to the true transition density n_t is obtained [21]. The procedures used to determine n_t include the dynamic method [5, 21, 22], the thermodynamic method [4, 23–25], and the random-phase approximation (RPA) [3]. In the following, the thermodynamic method will be employed, resulting with the constraint that determines the transition density given by the inequality [4]

$$C(n) = n^2 \frac{d^2 E_{\rm SNM}}{dn^2} + 2n \frac{dE_{\rm SNM}}{dn} + (1-2x)^2 \times \left[n^2 \frac{d^2 E_{\rm sym}}{dn^2} + 2n \frac{dE_{\rm sym}}{dn} - 2 \frac{1}{E_{\rm sym}} \left(n \frac{dE_{\rm sym}}{dn} \right)^2 \right] > 0 \,, \quad (3)$$

where n, $E_{\rm SNM}$, x and $E_{\rm sym}$, denote the baryon density, the energy per particle of symmetric nuclear matter, the proton fraction, and the symmetry energy, respectively. The transition density n_t is determined by solving the equation $C(n_t) = 0$, and the corresponding transition pressure reads $P_t(n_t, x_t) = P_b(n_t, x_t) + P_e(n_t, x_t)$, where P_b, P_e are the baryon and electron contributions, respectively. x_t denotes the proton fraction that corresponds to n_t, and is computed using the condition of β-equilibrium [4]. For the analysis of relationships between the transition density and pressure (n_t, P_t) and observables that characterize collective excitations in finite nuclei, we consistently employ a relativistic nuclear energy density functional (RNEDF) to compute the energy per particle of symmetric nuclear matter and the symmetry energy, and in the random phase approximation (RPA) calculation of strength functions in finite nuclei. In this work, the universal RNEDF with density-dependent meson–nucleon couplings (DD-ME) [26] is used, and excitations in spherical nuclei are analyzed in the relativistic quasiparticle random phase approximation (RQRPA) [27].

3. Constraining the symmetry energy parameters from collective excitations in nuclei

As the first step in the present analysis, we explore how various excitation modes in nuclei, that limit possible values of r_{np}, constrain the density dependence of the symmetry energy. Similar studies have recently been performed for different modes of excitation using the framework of energy density functionals (*e.g.* Refs. [29–31]). For the purpose of the present analysis, a consistent DD-ME set of RNEDFs that span a range of values $J = 30$–38 MeV and $L = 30$–110.8 MeV [32] is employed in a calculation of collective excitations. This set of RNEDFs was adjusted to accurately reproduce nuclear-matter properties, binding energies and charge radii of a standard set of spherical nuclei, but with constrained values for the symmetry energy J and slope parameter L [32]. These functionals were recently

used to constrain the density dependence of the nuclear symmetry energy and the neutron-skin thickness from the observed pygmy dipole strength (^{130,132}Sn) [33], and the anti-analog giant dipole resonance (^{208}Pb) [34].

By performing self-consistent relativistic mean-field calculations for nuclear ground states, and the corresponding RQRPA for collective excitations, we have computed the anti-analog giant dipole resonance (AGDR) and isovector giant quadrupole resonance (IVGQR) excitation energies in ^{208}Pb, the dipole polarizability $\alpha_{\rm D}$ of ^{208}Pb, and the pygmy dipole transition strength (PDR) in ^{68}Ni. For the set of RNEDFs, linear correlations are established between the calculated characteristics of collective excitations and the symmetry energy J and slope parameter L, in agreement with the results of the covariance analysis in Ref. [15]. By employing these correlations, together with the corresponding experimental results on the excitation strengths and energies, one can constrain the values of J and L. In Fig. 1, the resulting constraints of (J, L) values are shown, obtained from a comparison of the RNEDF (DD-ME) results and data on AGDR [48] and IVGQR [35] excitation energies (^{208}Pb), the dipole polarizability $\alpha_{\rm D}$ of ^{208}Pb [37], and the PDR energy weighted strength (^{68}Ni [38], ^{130,132}Sn [33]). For comparison, the results of a previous study are also shown, that was based on the same set of RNEDFs, but used data on the PDR in ^{130,132}Sn [33]. Figure 1 shows that all calculated excitation properties consistently constrain possible values of J and L, with differences attributed to variations of the experimental uncertainties. It is interesting to note that all results overlap in a narrow region of the (J, L) plane. The weighted average yields $J = 32.5 \pm 0.5$ MeV and $L = 49.9 \pm 4.7$ MeV. More accurate experimental results would, of course, further reduce the uncertainties shown in Fig. 1.

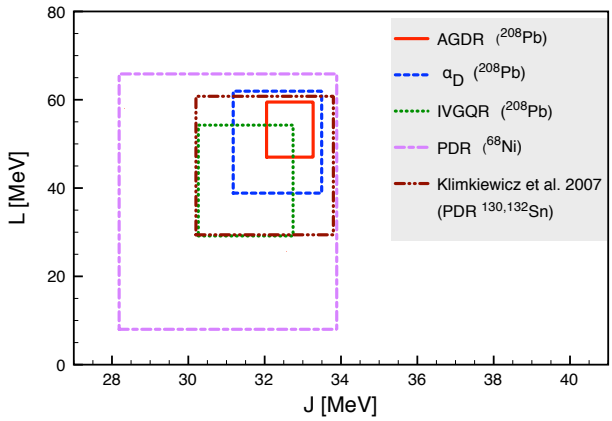

Fig. 1. Constraints of the symmetry energy at saturation J and the slope parameter L, obtained from a comparison of the RNEDF (DD-ME) results for various modes of excitation in nuclei with respective experimental data [33, 35, 37, 38, 48].

In Fig. 2, the weighted average values for the symmetry energy parameters (J, L) of the present analysis are compared with the constraints from a number of studies based on different methods and experimental data. These include constraints from heavy ion collisions (HIC) [30, 39–42], Quantum Monte Carlo (QMC) and neutron star study [43], nuclear binding energies (FRDM) [44], isobaric analog states (IAS) [45, 46], proton elastic scattering (^{208}Pb (p,p)) [47], pygmy dipole resonances (PDR) (LAND analysis for ^{130,132}Sn [33] and Carbone *et al.* analysis for ^{68}Ni and ^{132}Sn [29]). A detailed overview of various methods and respective references are given in Ref. [30]. In comparison to the previous studies, the present analysis provides rather stringent constraints on the symmetry energy parameters.

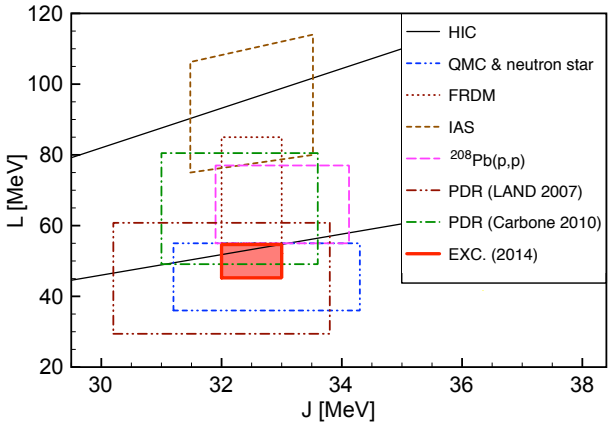

Fig. 2. (Color online) Constraints of the symmetry energy at saturation J and the slope parameter L, obtained from the analysis based on the RNEDF (DD-ME) and collective excitations in nuclei (denoted by EXC.), in comparison to various methods from previous studies (see the text and Ref. [30] for details).

4. Constraining the neutron star core-to-crust transition density and pressure from collective excitations in nuclei

In the following, we show the application of the RNEDF framework to determine the neutron star liquid-to-solid transition density and pressure. By employing the thermodynamic approach outlined in Sec. 2 (Eq. (3)), supplemented with the nuclear matter properties calculated using the RNEDF, the values of transition density n_{t} and pressure P_{t} are obtained. On the other side, the properties of various modes of excitation, already discussed in Sec. 3, are calculated in a self-consistent relativistic quasiparticle random phase approximation based on the same RNEDF (DD-ME). The same set of DD-ME effective interactions as in Sec. 3 is used in model calculations.

Figure 3 displays the calculated dipole polarizability $\alpha_{\rm D}$ in ^{208}Pb, as a function of the crust-to-core transition density $n_{\rm t}$, obtained using the set of DD-ME effective interactions spanning the range of values $J = 30$–38 MeV. From the calculated relationship between $\alpha_{\rm D}$ and $n_{\rm t}$ and the experimental value with uncertainties of the dipole polarizability [37], constraint on the range of values for $n_{\rm t}$ is obtained (see Fig. 3). This analysis is further extended to other modes of excitation, including AGDR, IVGQR, isovector spin monopole resonance (IVSMR) and pygmy dipole strength, to determine the values of both transition density and pressure. The overall result is displayed in Fig. 4, where the transition pressure $P_{\rm t}$ is plotted as a function of the transition density $n_{\rm t}$. The rectangles denote the values of $P_{\rm t}$ and $n_{\rm t}$, that in a consistent RQRPA calculation reproduce data on collective excitations within experimental uncertainties: the AGDR [34], IVGQR [35] and IVSMR [36] excitation energies (^{208}Pb), the dipole polarizability $\alpha_{\rm D}$ (^{208}Pb) [37], and the PDR energy weighted strength (^{68}Ni) [38]. One notices that collective excitations provide rather stringent constraints on the possible values of $P_{\rm t}$ and $n_{\rm t}$, and there is even a small region in the $(P_{\rm t}, n_{\rm t})$ plane in which all constraints overlap. Obviously, more accurate measurements of charge-exchange modes and pygmy dipole strength would further reduce the current uncertainties but, nevertheless, the weighted average from the present analysis yields $n_{\rm t} = 0.0955 \pm 0.0007$ fm^{-3} and $P_{\rm t} = 0.59 \pm 0.05$ MeV fm^{-3}. We note that in calculating these values we exclude the IVSMR because of considerable experimental errors of the currently available data.

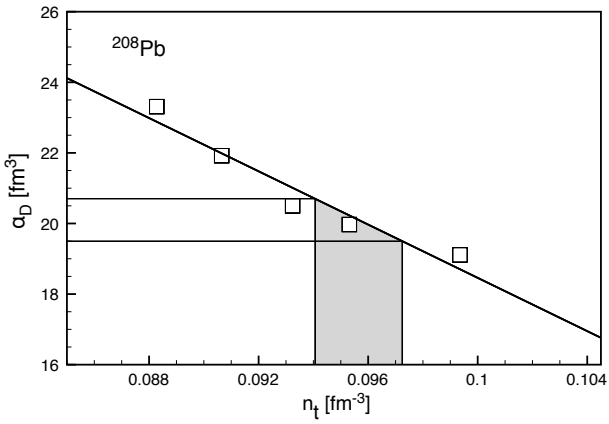

Fig. 3. The calculated dipole polarizability $\alpha_{\rm D}$ in ^{208}Pb shown as a function of the crust-to-core transition density $n_{\rm t}$. The experimental value with uncertainties for $\alpha_{\rm D}$ [37] and the corresponding constraint on $n_{\rm t}$ are also shown.

For comparison, Fig. 4 also includes constraints on (P_t, n_t) obtained by other methods, based on modified Gogny (MDI) interactions [5, 48], Dirac–Brueckner–Hartree–Fock (DBHF) calculations [49], and RNEDF with point couplings and constraints from the empirical range for the slope parameter L and neutron-skin thickness in Sn isotopes and ^{208}Pb [4]. A previous study based on the $A18+\delta v+\mathrm{UIX}^*$ interaction predicted a somewhat lower value for the transition density, $n_t = 0.087$ fm^{-3} [50], similar to recent work in the framework with realistic nucleon–nucleon and three nucleon interactions based on chiral effective field theory, $n_t = 0.076$–0.088 fm^{-3} [51]. The constraints obtained in the present analysis are consistent with the result based on the nonrelativistic microscopic equation of state of Friedman and Pandharipande [52]: $n_t = 0.096$ fm^{-3} [53].

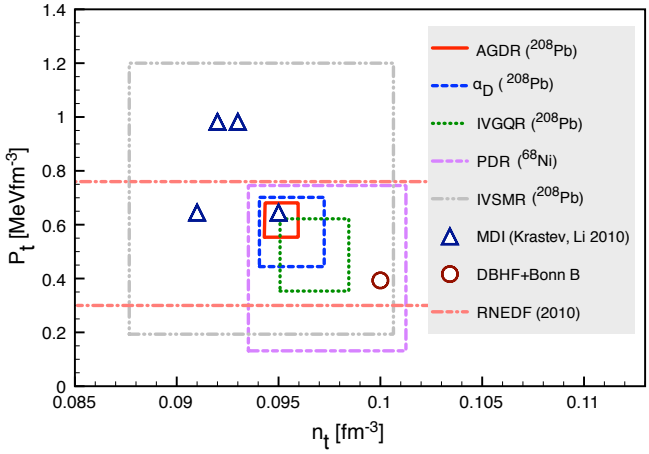

Fig. 4. The liquid-to-solid transition pressure P_t as a function of the transition density n_t calculated using the RNEDF (DD-ME) and experimental data for various excitation modes in nuclei (see the text for details). Results from previous studies include MDI [5, 48], DBHF+Bonn B interactions [49], and the RNEDF (point coupling) [4].

5. Conclusion

Collective excitations of finite nuclei provide important constraints on the density dependence of the symmetry energy and the properties of a neutron star crust. A set of RNEDFs characterized by systematic variation of the density dependence of the symmetry energy is used in a self-consistent calculations of the properties of various modes of excitation in nuclei. The thermodynamic method and the same set of RNEDFs determine the phase transition density n_t and pressure P_t at the inner edge between the liquid

core and the solid crust of a neutron star. By comparing the RNEDF values on collective excitations in nuclei with experimental data, rather stringent constraints on the possible values for (P_t, n_t) are obtained. Future progress in experimental studies with reduced experimental uncertainties of observables that characterize collective modes of excitation will further constrain the structure of the neutron star crust.

This work was supported by the Marie Curie FP7-PEOPLE-2011-COFUND program NEWFELPRO and the Swiss National Science Foundation. N.P. acknowledges support by the Polish Academy of Sciences to present this work at the Zakopane Conference on Nuclear Physics 2014.

REFERENCES

[1] J.M. Lattimer, M. Prakash, *Phys. Rep.* **333**, 121 (2000).
[2] P. Haensel, A.Y. Potekhin, D.G. Yakovlev, *Neutron Stars 1: Equation of State and Structure*, Springer-Verlag, New York 2007.
[3] C.J. Horowitz, J. Piekarewitz, *Phys. Rev. Lett.* **86**, 5647 (2001).
[4] Ch.C. Moustakidis *et al.*, *Phys. Rev.* **C81**, 065803 (2010).
[5] J. Xu, L.W. Chen, B.A. Li, H.R. Ma, *Astrophys. J.* **697**, 1549 (2009).
[6] C. Ducoin, J. Margueron, C. Providencia, I. Vidana, *Phys. Rev.* **C83**, 045810 (2011).
[7] A.W. Steiner, M. Prakash, J.M. Lattimer, P.J. Ellis, *Phys. Rep.* **411**, 325 (2005).
[8] J. Carriere, C.J. Horowitz, J. Piekarewicz, *Astrophys. J.* **593**, 463 (2003).
[9] C.J. Horowitz, J. Piekarewicz, *Phys. Rev.* **C66**, 055803 (2002).
[10] F.J. Fattoyev, J. Piekarewicz, *Phys. Rev.* **C82**, 025810 (2010).
[11] F.J. Fattoyev, J. Piekarewicz, *Phys. Rev.* **C86**, 015802 (2012).
[12] S. Abrahamyan *et al.*, *Phys. Rev. Lett.* **108**, 112502 (2012).
[13] C.M. Tarbert *et al.*, *Phys. Rev. Lett.* **112**, 242502 (2014).
[14] B. Klos *et al.*, *Phys. Rev.* **C76**, 014311 (2007).
[15] N. Paar *et al.*, *Phys. Rev.* **C90**, 011304(R) (2014).
[16] D. Savran, T. Aumann, A. Zilges, *Prog. Part. Nucl. Phys.* **70**, 210 (2013).
[17] B.-A. Li, L.-W. Chen, C.M. Ko, *Phys. Rep.* **464**, 113 (2008).
[18] R.J. Furnstahl, *Nucl. Phys.* **A706**, 85 (2002).
[19] M. Centelles, X. Roca-Maza, X. Vinas, M. Warda, *Phys. Rev. Lett.* **102**, 122502 (2009).
[20] F.J. Fattoyev, J. Piekarewicz, *Phys. Rev.* **C84**, 064302 (2011).

[21] C.J. Pethick, D.G. Ravenhall, C.P. Lorenz, *Nucl. Phys.* **A584**, 675 (1995); F. Douchin, P. Haensel, *Phys. Lett.* **B485**, 107 (2000).
[22] C. Ducoin, Ph. Chomaz, F. Gulminelli, *Nucl. Phys.* **A789**, 403 (2007).
[23] J.M. Lattimer, M. Prakash, *Phys. Rep.* **442**, 109 (2007).
[24] S. Kubis, *Phys. Rev.* **C76**, 025801 (2007).
[25] A. Worley, P.G. Krastev, B.A. Li, *Astrophys. J.* **685**, 390 (2008).
[26] T. Nikšić *et al.*, *Phys. Rev.* **C66**, 024306 (2002).
[27] N. Paar *et al.*, *Rep. Prog. Phys.* **70**, 691 (2007).
[28] X. Roca-Maza, N. Paar, G. Coló, to appear in *J. Phys. G* (2014).
[29] A. Carbone *et al.*, *Phys. Rev.* **C81**, 041301(R) (2010).
[30] M.B. Tsang *et al.*, *Phys. Rev.* **C86**, 015803 (2012).
[31] X. Roca-Maza *et al.*, *Phys. Rev.* **C87**, 034301 (2013).
[32] D. Vretenar *et al.*, *Phys. Rev.* **C68**, 024310 (2003).
[33] A. Klimkiewicz *et al.*, *Phys. Rev.* **C76**, 051603(R) (2007).
[34] A. Krasznahorkay *et al.*, `arXiv:1311.1456 [nucl-ex]`.
[35] S.S. Henshaw *et al.*, *Phys. Rev. Lett.* **107**, 222501 (2011).
[36] T. Wakasa *et al.*, *Phys. Rev.* **C85**, 064606 (2012).
[37] A. Tamii *et al.*, *Phys. Rev. Lett.* **107**, 062502 (2011).
[38] O. Wieland *et al.*, *Phys. Rev. Lett.* **102**, 092502 (2009).
[39] M.B. Tsang *et al.*, *Phys. Rev. Lett.* **92**, 062701 (2004).
[40] M. Famiano *et al.*, *Phys. Rev. Lett.* **97**, 052701 (2006).
[41] T.X. Liu *et al.*, *Phys. Rev.* **C76**, 034603 (2007).
[42] Z.Y. Sun *et al.*, *Phys. Rev.* **C82**, 051603(R) (2010).
[43] A.W. Steiner, S. Gandolfi, *Phys. Rev. Lett.* **108**, 081102 (2012).
[44] P. Möller, W.D. Myers, H. Sagawa, S. Yoshida, *Phys. Rev. Lett.* **108**, 052501 (2012).
[45] P. Danielewicz, J. Lee, *AIP Conf. Proc.* **1423**, 29 (2012).
[46] P. Danielewicz, J. Lee, *Nucl. Phys.* **A818**, 36 (2009).
[47] J. Zenihiro *et al.*, *Phys. Rev.* **C82**, 044611 (2010).
[48] P.G. Krastev, B.A. Li, `arXiv:1001.0353 [astro-ph.SR]`.
[49] F. Sammarruca, P. Liu, *Phys. Rev.* **C79**, 057301 (2009).
[50] A. Akmal, V.R. Pandharipande, D.G. Ravenhall, *Phys. Rev.* **C58**, 1804 (1998).
[51] K. Hebeler, J.M. Lattimer, C.J. Pethick, A. Schwenk, *Astrophys. J.* **773**, 1 (2013).
[52] B. Friedman, V.R. Pandharipande, *Nucl. Phys.* **A631**, 502 (1981).
[53] C.P. Lorenz, D.G. Ravenhall, C.J. Pethick, *Phys. Rev. Lett.* **70**, 379 (1993).